Proceedings of the 5th International Conference on Fluid Flow and Thermal Science (ICFFTS 2024)
Lisbon, Portugal- November 21 - 23, 2024
Paper No. 153
DOI: 10.11159/icffts24.153

Numerical and Experimental Study on the Transitional Heat Transfer of a Vertical Tall Square Aluminum Tube

Cheng-Pu Yang[1], Shwin-Chung Wong[1]
[1]National Tsing Hua University, Department of Power Mechanical Engineering
101 Section 2, Kuan-Fu Road, Hsin-Chu City, Taiwan
apuapu@gapp.nthu.edu.tw; scwong@pme.nthu.edu.tw

Abstract –The purpose of this study is to develop turbulence-enhanced heat dissipation fins for natural convection from a large-scale vertical square tube, with the expectation of future applications in large-scale electric devices such as the cooling electric vehicle charging poles. To provide reference data for future research, this study first involves conducting experiments to measure the total surface heat rate of a closed aluminium square tube under a temperature difference of approximately 55°C. The experimental data will then be compared with various turbulence models. Additionally, the simulation will compare the velocity and temperature at the inlet, middle, and outlet sections of the tube, using the LES model as a benchmark. The results show that the $k-kl-\omega$ model most closely matches the LES model in terms of velocity and temperature distribution across all sections. Although the LES model differs from the experimental data by 13%, the $k-kl-\omega$ model remains the most consistent with the LES model in terms of the total surface heat transfer rate. These results will provide significant guidance for optimizing fin spacing and structural design for large-scale electric devices in future studies.

***Keywords*:** natural convection, transitional flow, turbulence, heatsink, closed-duct heatsink

1. Introduction

Natural convection is preferred as a fundamental passive heat transfer method whenever feasible, due to its inherent simplicity, high reliability, and cost-effectiveness. Owing to these advantages, natural convection heat transfer is utilized in heat exchange applications, such as the cooling of electronic devices and passive solar heating [1–2], etc. In common electronic applications, although the traditional U-shaped vertical plate-fin heatsinks are mostly used, the vertical closed-duct heatsink is also adopted. Its heat dissipation performance is often superior to that of a traditional plat-fin heatsink due to the existence of the chimney effect. For example, the industrial computer Airtop, by the Israeli company Compulab, adopts vertical closed-duct heatsinks on both sides of the casing, claiming a 200 W heat dissipation capacity, currently the highest for fanless personal computers. To gain a higher heat convection coefficient, it is possible for a tall closed-duct heatsink, with a larger optimum fin spacing (S_{opt}), to exhibit a transitional flow field from laminar to turbulent. These large-scale heatsinks are expected to be effectively used in outdoor environments requiring minimal maintenance while still reaching significant heat dissipation, such as for cooling electric vehicle charging poles.

In recent decades, numerous studies have investigated various characteristics of natural convection. Elenbaas [3] was the pioneer in studying the effects of natural convection from vertical isothermal plates. His experiments used a pair of parallel square plates to obtain the average heat convection coefficient (h) associated with 2-D isothermal parallel plates at different spacings (S). Following his work, a series of extensive experimental and simulation studies have been performed on natural convection laminar flow from heatsinks. Refs. [4–13] display only a few of them. Aihara [4–5] indicated that the heat convection coefficient decreased as the fin spacing shortened in plate-fin channels and vertical closed ducts. Bar-Cohen and Rohsenow [6] proposed a theoretical asymptotic approach to obtain an equivalent semi-empirical correlation by empirically combining the analytical solutions of the two extreme fully-developed flow ($S\rightarrow 0$) and single-plate flow ($S\rightarrow\infty$). Floryan and Novak [7] numerically studied multi-channel effects. For two-channel and three-channel conditions, a recirculation zone formed by the outside walls near the entrance when Gr was sufficiently large. This would decrease the heat transfer rate of the multi-channels. In contrast, no recirculation zone would appear for infinite channels, leading to significantly over-estimated heat transfer rates. Vollaro et al. [8] utilized the assumptions and the S_{opt} correlations of Bar-Cohen and Rohsenow [6], as well as radiation considerations, to conduct the optimum design for natural-convection vertical plate-fin heatsinks. It is noted that assumptions of Bar-Cohen and Rohsenow [6] omitted the viscous effects at the corners. Wong and Chu [9]

indicated that the external buoyancy caused by the hot air zone above the heatsink provides significant virtual chimney effect, while the recirculation zones entrance near the outside-channel entrance provide a negative effect.

For actual plate-fin heatsinks under the vertical orientation, Welling and Wooldridge [10] tested heatsinks with different geometric parameters. Aihara [11] experimentally measured the convection heat transfer coefficient and indicated that the main differences among the plate-fin heatsinks and parallel plates come from the stagnant corner effect. He suggested the stagnant corner effect becomes less than 5% as $L_f/S > 5$. Thus, for long fins with $L_f/S > 5$, the heatsinks can be simulated as parallel plates. Van de Pol and Tierney [12] proposed an empirical formula for h according to the data of Welling and Wooldridge [10] for short-fin heatsinks $\left(L_f / S < 4, L_f / H < 0.094\right)$. Leung et al. [13] experimentally studied the vertical plate-fin heatsinks and indicated the S_{opt} of 10±1 mm for a 250 mm tall plate-fin heatsink with L_f = 60 mm, approximating the predicted value of 8.5 mm based on the Bar-Cohen and Rohsenow's correlation for S_{opt} [6].

For closed-duct part, the data of Elenbaas [14] indicated that, at the same $\frac{r}{h}Gr_{r,w}Pr$, the square duct shows a highest Nu among rectangular closed ducts. Ramakrishna et al. [15] numerically studied the isothermal square ducts with consistent results as Elenbaas [14]. They further proposed an empirical formula for natural convection from vertical isothermal square ducts. Lee [16] investigated the natural convection heat and mass transfer from vertical square ducts. Aihira [17] and Raithby and Hollands [18] modified the scale length of Elenbaas [13]. Their modifications yielded excellent agreement with Elenbaas' data [13] at very small and very large Ra', but with 25% error at the transitional region. In the simulation part, Yovanovich and Muzychka [19] proposed an improved empirical formula (1) using $\sqrt{A}$ as the characteristic length for natural-convection vertical closed-duct heatsinks with different cross-sectional shapes.

$$Nu_{\sqrt{A}} = \left\{ \left[2\frac{Ra_{\sqrt{A}}(\sqrt{A}/L)}{fRe_{\sqrt{A}}}\left(\frac{\sqrt{A}}{P}\right)2 \right]^{-n} + \left[0.6\left(Ra_{\sqrt{A}}\frac{\sqrt{A}}{L}\right)^{\frac{1}{4}} \right]^{-n} \right\}^{-1/n} \quad (1)$$

Eq. (1) shows that, under the same $Ra_{\sqrt{A}}\sqrt{A}/L$, a square pipe with an aspect ratio of 1.0 achieves the highest $Nu_{\sqrt{A}}$.

Most of the literature relevant to natural convection primarily focuses on laminar flow because laminar flow exists in the adopted small-scale heatsinks. From Eq. (2) [3], H is proportional to S^4.

$$Ra' \equiv \frac{S}{H}Ra = \frac{S^3 g\beta(T_w - T_\infty)}{H \nu\alpha} \quad (2)$$

Therefore, S increases for larger H. Thus, we may increase Ra' to enlarge Nu by letting the flow field to reach the transition flow or turbulence flow. If external stimulating, such as surface roughening or adding a stimulus, is excluded, this aim may be realized in a tall, large-scale heatsink. However, current analyses of natural-convection transitional or turbulent flow are predominantly focused on vertical flat plates. Studies on transitional or turbulent flow in vertical isothermal closed ducts remain insufficient. Also, experimental data on the transitional or turbulent flow field characteristics, including the distributions of velocity, temperature, and turbulent kinetic energy, are limited. Yilmaz et al. [20] conducted a comprehensive comparison between the experimental data and the simulation results for turbulent flow. Afterward, Abdollahzadeh et al. [21] conducted a turbulent analysis of a two-dimensional vertical plate and compared various RANS turbulence models with the experimental results of Yilmaz et al. [20]. They indicated that the RNG k-ε and low-Re k-ε models closely matched the experimental data for the inlet velocity, while the low-Re k-ε model was more accurate for the outlet velocity [22], although the agreements of all the RANS models are far worse than the Large-Eddy-Simulation (LES) which closely resemble the direct numerical simulation (DNS) [23].

This study aims to determine whether these RANS turbulence models can produce reliable results when simulating a vertical closed-duct heatsink with an isothermal wall temperature. An LES analysis will also be conducted as a comparison basis, as LES closely resembles DNS data for turbulent flow [23]. We will examine the steady-state heat transfer characteristics and performance of a vertical closed-duct heatsink in the transitional range both experimentally and numerically. Experimentally, we will measure the temperature characteristics of a single closed-duct square aluminium alloy tube with L = 52 mm, S = 52 mm, and H = 1800 mm (Fig. 1). This study focuses on evaluating the performance of the turbulence models in a single square closed duct; therefore, the S_{opt} is not the primary focus of this research. Numerically, a symmetrical simulation domain is considered to reduce the computational load. Thus, we aim to collect experimental and simulation data as references for future study on a large-scale closed-duct heatsink.

2. Experimental setup

To obtain the total heat transfer rate of the heatsink, measurements were taken once the heatsink reached a uniform temperature and the heating temperature stabilized at approximately 55 °C above the ambient temperature (25 °C). This allowed the total heat transfer rate to be determined from the power supply, with 19 temperature points set at the base plate of the heatsink using K-type thermocouples (Omega, Inc.). In natural convection, heat radiation plays a crucial role. Therefore, the heatsink surfaces were sprayed with a thin layer of thermal radiation correction paint with an emissivity of 0.95 (Note: This value has been ensured using K-type thermocouples.). During the experiment, heat loss occurred at the heating zone, so a 10 mm thick Bakelite® plate was added at the back to reduce the loss. The heating zone utilized polyimide film for heating and transferred the heat evenly to the heatsink through a thermal pad. The heatsink material was Al 6061, with a thermal conductivity of approximately 200 W/(m·K). To reach a steady state, measurements were started after 5 h, when the temperature variations at each point did not exceed ±0.1°C.

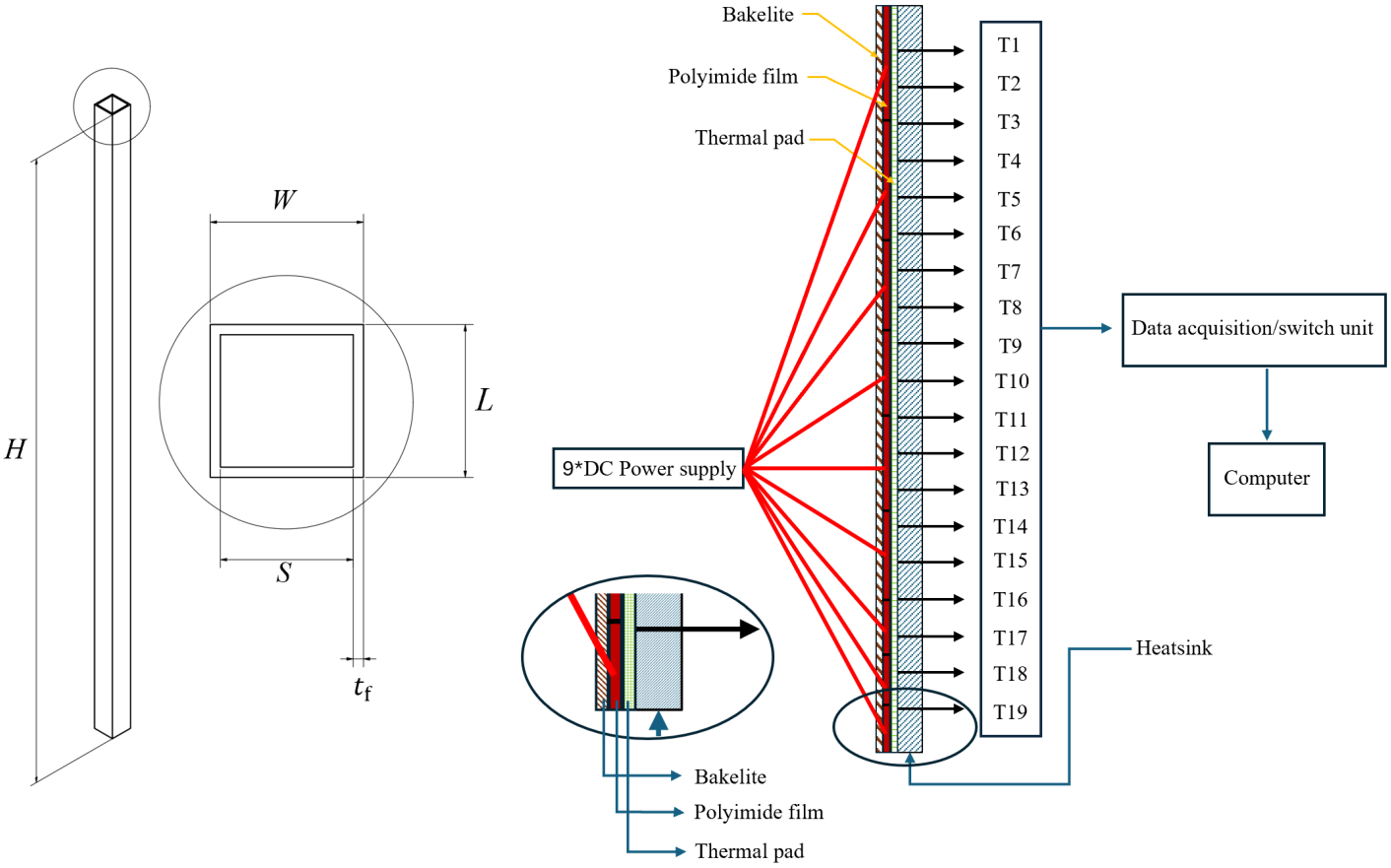

Fig. 1 Dimensions and test arrangement for a large-scale closed-duct heatsink.

3. Numerical setup

The numerical simulation was conducted using the commercial CFD software ANSYS Fluent® 2022 R2. Experiments lasting more than 5 h were considered to be in a steady state. Therefore, steady-state simulations were used. The pressure-velocity coupling is handled using the Coupled algorithm. Body-force weighting was used for the pressure term. Second-order upwind spatial discretization was applied to the convective terms of the momentum, energy, and turbulence transport equations. Gradients were evaluated using the Least Squares Cell-Based method. A residual target value of 10^{-9}

was set as the criterion for iterative convergence for all equations. Since the temperature difference between the heating temperature and the ambient temperature exceeded 50 °C, the air was modeled as a compressible ideal gas. The governing equations are as follows:

$$\nabla \cdot (\rho \vec{V}) = 0 \tag{3}$$

$$(\rho \vec{V} \cdot \nabla) \vec{V} = -\nabla P + \rho g + \mu(\nabla^2 \vec{V}) \tag{4}$$

$$\nabla (\rho T) = \nabla \cdot (\rho \alpha \nabla T) \tag{5}$$

As shown in Fig. 3, the simulation domain needs to be extended to account for the virtual chimney effect, based on the results of Wong and Chu [9]. A symmetrical simulation domain is used to reduce the computational load. For the mesh shown in Fig. 4, since the *k–ω* SST model was used, the grid *y*+ near the wall was kept below 1 to ensure data accuracy.

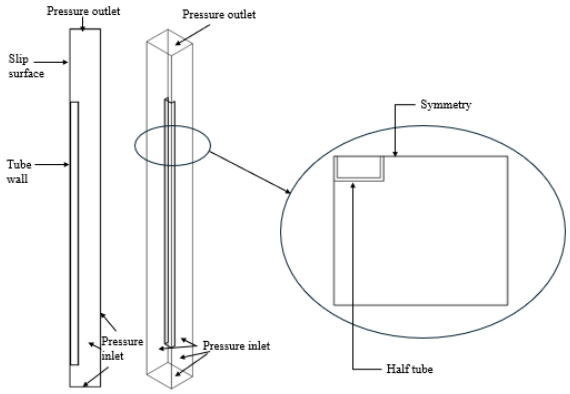

Fig. 2 Simulation domain

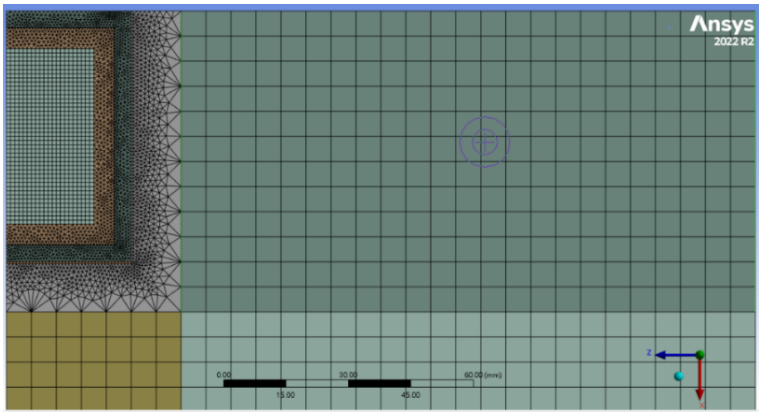

Fig. 3 Grid section.

3.1 Turbulence Models

This study used five turbulence models to simulate the fluid field and heat transfer. The results of the velocity and temperature were then compared. The features of each turbulence model are as follows:

RNG $k-\varepsilon$ is an improved version of the $k-\varepsilon$ model that handles the energy dissipation of turbulence through statistical renormalization. The standard wall function is suitable for high-*Re* flows and can use larger grid sizes near the wall.

Realizable $k-\varepsilon$ ewt (enhances wall treatment) improves the $k-\varepsilon$ model with modified turbulent eddy viscosity and turbulent kinetic energy dissipation rate equation. Enhanced wall treatment provides more accurate predictions of wall shear and heat transfer by selecting different processing methods based on varying *y*+ values.

SST $k-\omega$ model combines the $k-\omega$ and the $k-\varepsilon$ approaches. It uses $k-\omega$ near the wall to process fine structures and $k-\varepsilon$ to handle free shear flow away from the wall. The near-wall processing for low *Re* has been further improved, making it suitable for low-*Re* flow conditions.

The $k-kl-\omega$ model is specifically designed to simulate the laminar-turbulent transition process. It employs three turbulence parameters: *k*, representing the turbulent kinetic energy; *kl*, representing the laminar kinetic energy; and ω, representing the specific dissipation rate. The transport equations for the $k-kl-\omega$ model are as follows:

$$\frac{Dk}{Dt} = P_k + R + R_{NAT} - \omega k - D_T + \frac{\partial}{\partial x_j}\left[\left(\nu + \frac{\alpha_T}{\alpha_K}\right)\frac{\partial k}{\partial x_j}\right]$$

$$\frac{Dk_L}{Dt} = P_{K_L} + R + R_{NAT} - D_L + \frac{\partial}{\partial x_j}\left[\nu\frac{\partial k_L}{\partial x_j}\right]$$

$$\frac{D\omega}{Dt} = C_{\omega 1}\frac{\omega}{k}P_{k_T} + \left(\frac{C_{\omega R}}{f_W} - 1\right)\frac{\omega}{k}\left(R + R_{NAT}\right) - C_{\omega 2}\omega^2 + C_{\omega 3}f_\omega \alpha_T f_W^2 \frac{\sqrt{k_T}}{d^3} + \frac{\partial}{\partial x_j}\left[\left(\nu + \frac{\alpha_T}{\alpha_\omega}\right)\frac{\partial \omega}{\partial x_j}\right]$$

This model captures the details of the transition from laminar to turbulent boundary layers, providing more accurate predictions of the transition region.

Large Eddy Simulation (LES) is a turbulence model that directly simulates large-scale eddy structures in turbulence while handling small-scale turbulence using a subgrid-scale model, thus reducing computational costs. Even so, it is rather time consuming, requiring 16 days for a single case, while the other models only need about 2 h for a case. According to the results of Chatzikyriakou et al. [23], LES can closely match experimental data. Therefore, LES is an important indicator in this study.

3.2 Boundary Conditions

The boundary conditions of the simulation utilize the experimental data, with the temperatures of the 19 measurement points averaged to determine the base plate temperature. The total heat transfer rate of the heatsink is simulated under fixed ambient temperature and heatsink base temperature conditions. The average temperature of the 19 measurement points is 355.66 K, while the ambient temperature of the experiment is 299.19 K. Given the ambient temperature, the corresponding air density is 1.179844 kg/m³.

3.3 Computation of Experimental Q_{loss}

For the isothermal heatsink base, we only need to simulate the experimental Q_{loss} through the back side of the system, as shown in Fig. 4. At the back side of the system, a few wood plates separated the space, forming several laminar circulation zones. With 8 screws used to tighten the Bakelite® plates, the polyimide heating film and the thermal pad layer, the contact resistances were ignored in the analysis. This might cause slight uncertainty of Q_{loss} and the differences between the model predictions and the experimental heat transfer rate, as will be discussed in Section 4.

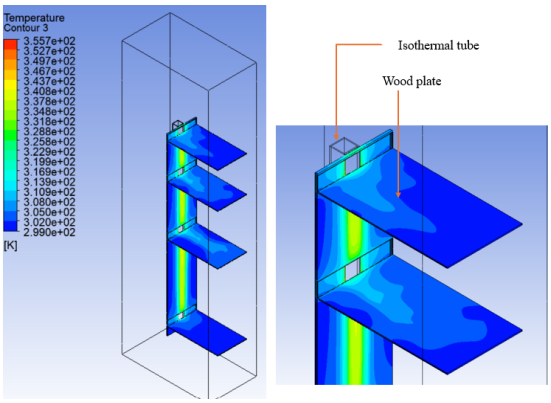

Fig. 4 The computation domain and boundary conditions to predict experimental Q_{loss}.

4. Results and Discussion

As observed in Figs. 5, 6, and 7, the $k-\omega$ and $k-kl-\omega$ models closely resemble the flow field distribution of the reference LES model, with the $k-kl-\omega$ model showing the highest similarity. A similar pattern is observed in the temperature profiles shown in Figs. 8, 9, and 10. This is because the $k-\omega$ and $k-kl-\omega$ models provide a more detailed description of near-wall behavior compared to the $k-\varepsilon$ model, making them more consistent with LES when examining both velocity and temperature contours. The $k-kl-\omega$ model, in particular, captures the flow field more accurately because it includes kl, which represents laminar kinetic energy. This addition allows for a more precise description of the natural convection process, as the flow transitions from the laminar phase and ultimately becomes turbulent. As a result, the $k-kl-\omega$ model more closely aligns with LES in both temperature and velocity profiles.

Figs. 11 and 12 respectively show the longitudinal velocity and temperature contours for different models. Although the LES model, as well as a few other models, appears to predict the acceleration of the flow after exiting the tube, which is anticipated as a result of the virtual chimney effect [9], not every model does. This puzzle will be investigated in the future.

In Table 1, we listed the predicted values of Q and the experimental Q_{loss}. Actually, 8 screws were used to tighten the Bakelite® plate, the polyimide heating film and thermal pad layer. Consequently, little discrepancy may exist in calculating Q_{loss}, which could lead to little difference between the predicted Q and the experimental Q (calculated as predicted Q/(measured Q – predicted Q_{loss})). Further investigation is needed to clarify why the predicted Q using the LES model would be smaller than the measured Q by 13%.

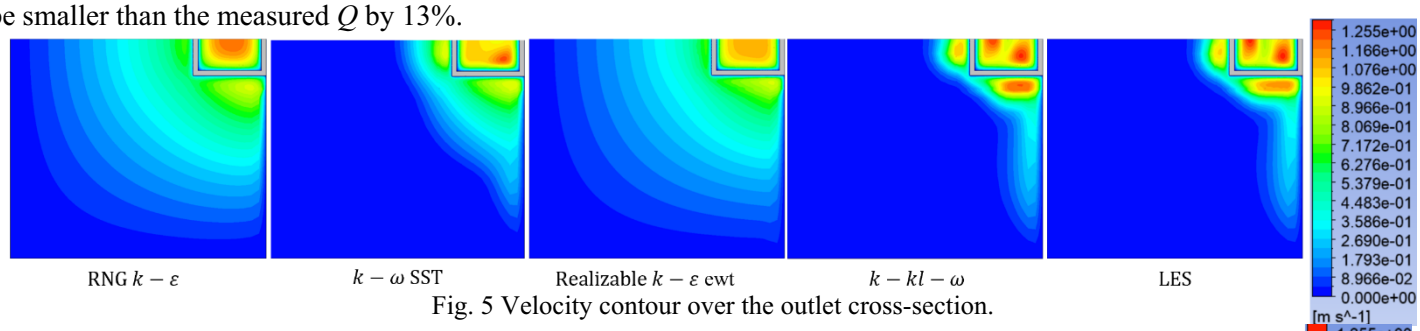

Fig. 5 Velocity contour over the outlet cross-section.

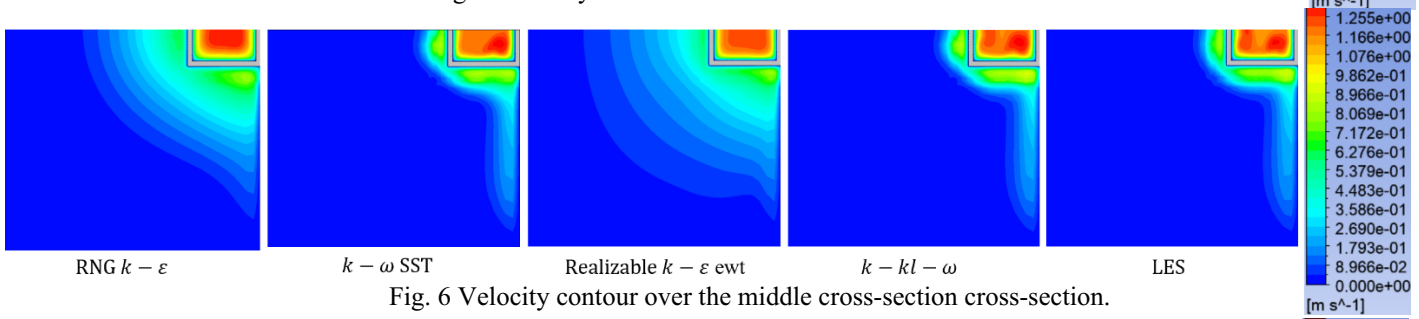

Fig. 6 Velocity contour over the middle cross-section cross-section.

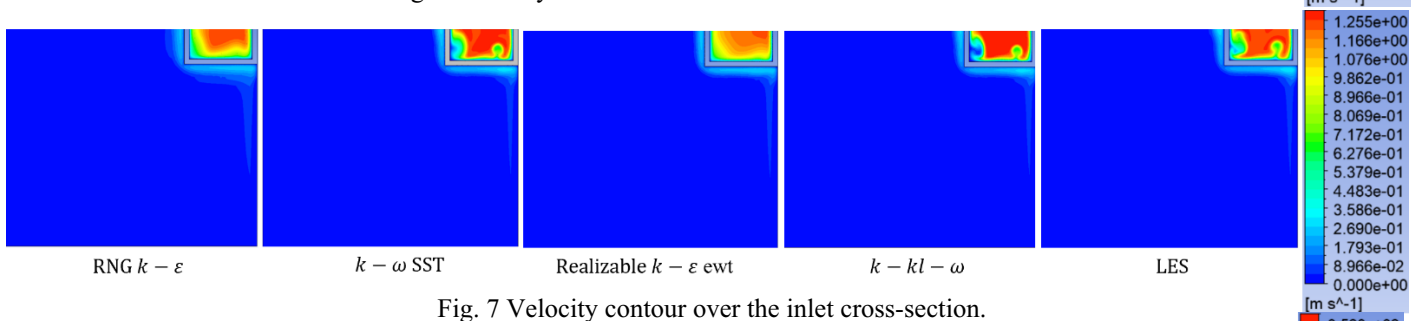

Fig. 7 Velocity contour over the inlet cross-section.

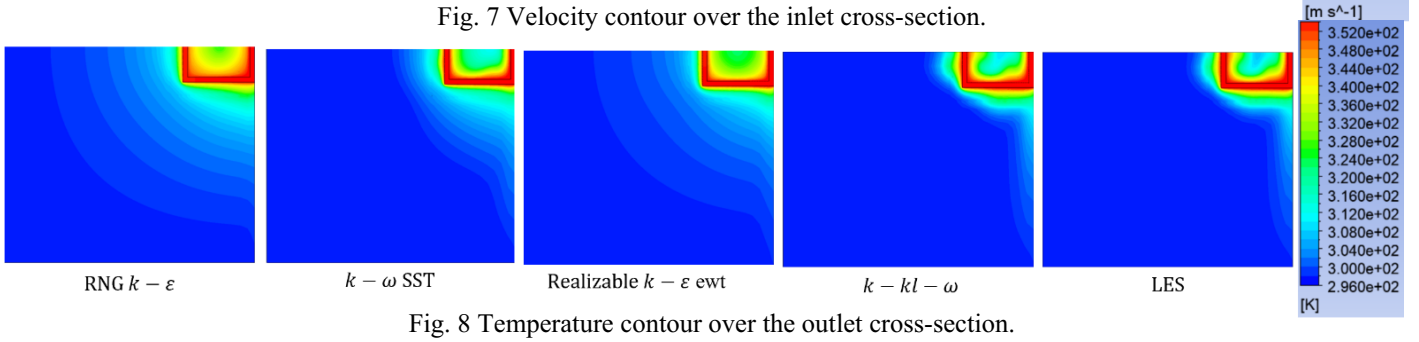

Fig. 8 Temperature contour over the outlet cross-section.

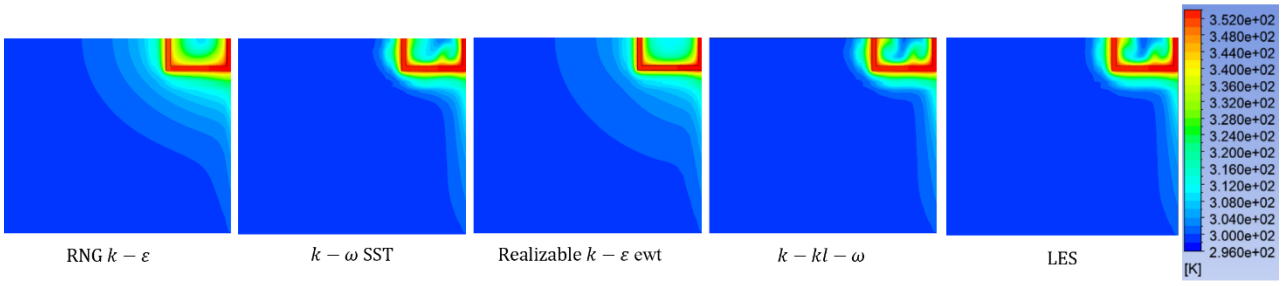

Fig. 9 Temperature contour over the middle cross-section.

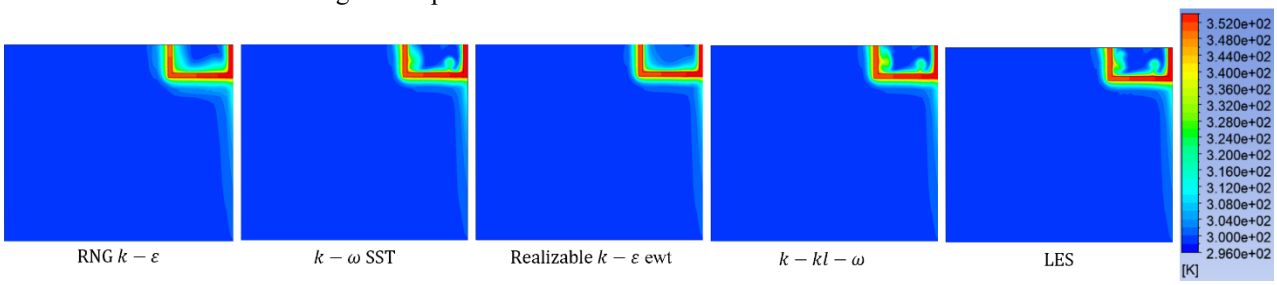

Fig. 10 Temperature contour over the inlet cross-section.

In the longitudinal section, the hot air accelerates after exiting the closed tube due to the virtual chimney effect. However, none of the four models closely match the LES model in terms of velocity or temperature, and the reasons for these discrepancies will need to be explored in future research. This study also compares the total heat transfer rates obtained from numerical simulations with the experimental data. In the experimental data, a predicted Q_{loss} of 21W must be subtracted when compared with the computational results to ensure accuracy. As shown in Table 1, although there is a 13% discrepancy between the LES and experimental data, LES is used as the benchmark for comparison because it closely approximates DNS simulations [23]. Among all the models, $k-kl-\omega$ is the closest to LES in terms of total heat transfer rate, which will greatly aid our subsequent research. In the future, we will use the $k-kl-\omega$ model to find, due to its faster calculations, the optimal gap of a partially-open duct heatsink which presents higher heat transfer rates.

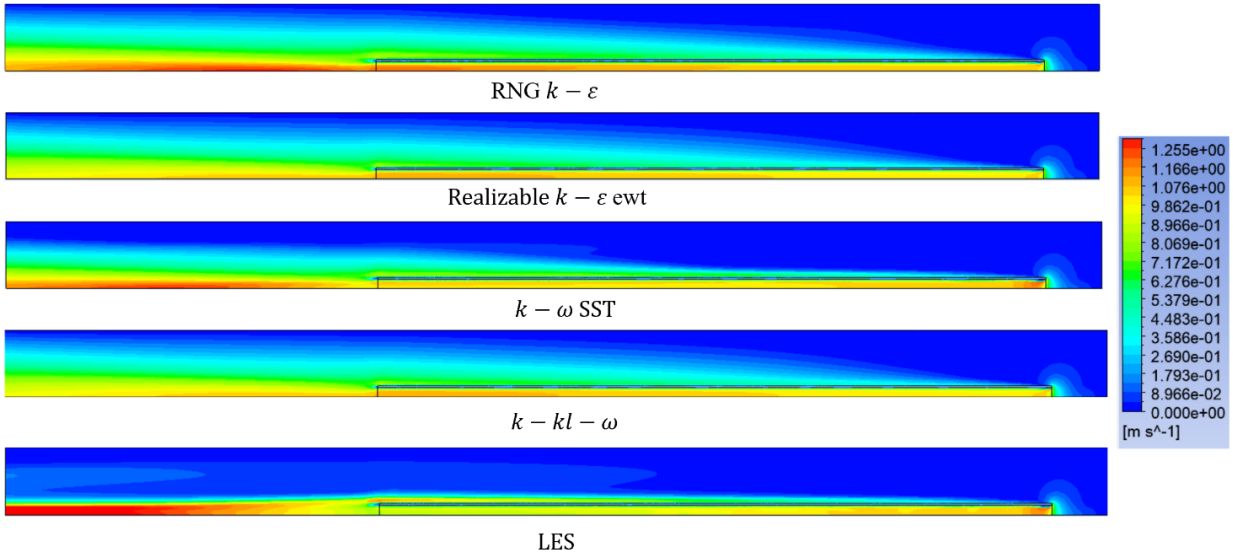

Fig. 11 Longitudinal velocity contours along the central section of the tube for different models.

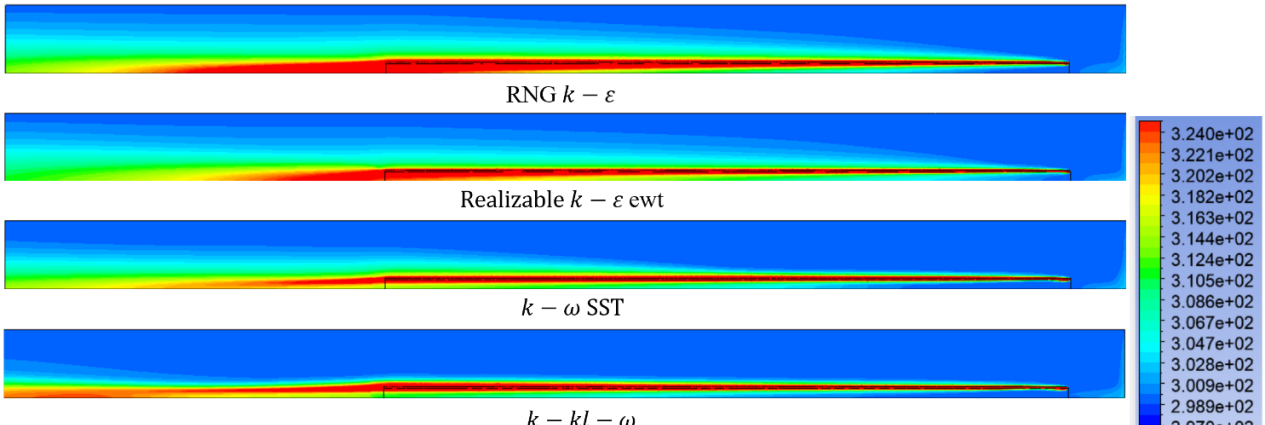

Fig. 12 Longitudinal temperature contours along the middle section of the half tube for different models.

Table 1: Comparison of total heat transfer rates for various turbulence models with the experimental measurement.

Turbulence model	Predicted Q (W)	Predicted Q_{loss} (W)	Measured Q (W)	error
RNG $k-\varepsilon$	330.43	21	322.01	-10%
$k-\omega$ SST	268.74			11%
Realizable $k-\varepsilon$ ewt	287.31			5%
$k-kl-\omega$	264.76			12%
LES	262.94			13%

Conclusion

The purpose of this study is to develop turbulence-enhanced heat dissipation fins for natural convection from a large-scale vertical square tube. To provide reference data for future research, it is necessary to compare the performance of a closed aluminium tube under different turbulence models with the LES results and experimental data.

The computational results indicate that among all turbulence models, the $k-kl-\omega$ model is particularly suitable for this study. This is because the kl term accounts for the transition from laminar to turbulent flow in natural convection and considers the near-wall flow conditions. The $k-kl-\omega$ model closely matches the LES benchmark in both velocity and temperature profiles. Finally, a comparison of the predicted total heat transfer rates of all the models and the experimental data shows that the LES model differs from the experimental data by 13%, while the $k-kl-\omega$ model differs from the LES model by only 1%. This study enhances our understanding of how to use computationally efficient and faster RANS model in future estimation of the optimal gap for a novel partially-open duct heatsink for enhanced cooling of large-scale electric devices, such as the electric vehicle charging poles.

References

[1] S. Feng, M. Shi, H. Yan, S. Sun, F. Li, and T.J. Lu, "Natural convection in a cross-fin heat sink," *Appl. Therm. Eng*. Vol. 132, no. 3, pp. 30–37, 2018.

[2] S.H. Yu, K.S. Lee, and S.J. Yook, "Natural convection around a radial heat sink," *Int. J. Heat Mass Transf*, vol. 53 pp. 2935–2938, 2010.

[3] W. Elenbaas, "Heat dissipation of parallel plates by free convection," *Physica*, vol. 9, pp. 1–28, 1942.

[4] T. Aihara, "Natural convection heat transfer from vertical rectangular-fin arrays: Part 3, heat transfer from fin-flats," *Bulletin of JSME*, vol. 13, pp. 1192–1200, 1970.

[5] T. Aihara, Natural convection heat transfer from vertical rectangular-fin arrays: Part 2, heat transfer from fin-edges, *Bull. JSME*, vol. 13, pp. 1182–1191, 1970.

[6] A. Bar-Cohen and W.M. Rohsenow, "Thermally optimum spacing of vertical, natural convection cooled, parallel plates," *ASME J. Heat Transf.* vol. 106, pp. 116–123, 1984.

[7] J.M. Floryan and M. Novak, "Free convection heat transfer in multiple vertical channels," *Int. J. Heat Fluid Flow*, vol. 1, no. 4, pp. 244–253, 1995.

[8] A.D. Vollaro, S. Grignaffini, and F. Gugliermetti, “Optimum design of vertical rectangular fin arrays,” *Int. J. Therm. Sci*. vol. 38, no. 6, pp. 525–529, 1999.
[9] S.-C. Wong and S.-H. Chu, “Revisit on natural convection from vertical isothermal plate arrays–effects of extra plume buoyancy,” *Int. J. Therm. Sci*. vol. 120, pp. 263–272, 2017.
[10] J.R. Welling and C.B. Wooldridge, “Free convection heat transfer coefficients from rectangular vertical fins,” *ASME J. Heat Transf.* vol. 87, no. 4, pp. 439–444, 1965.
[11] T. Aihara, “Natural convection heat transfer from vertical rectangular profile,” *JSME*, vol. 34, pp. 915–926, 1968.
[12] D.W. Van de Pol and J.K. Tierney, “Free convection Nusselt number for vertical U-shaped channels,” *ASME J. Heat Transf.* vol. 95, no. 4, pp. 542–543, 1973.
[13] C.W. Leung, S.D. Probert, M.J. Shilston, “Heat exchanger: optimal separation for vertical rectangular fins protruding from a vertical rectangular base,” *Appl. Energy,* vol. 19, no. 2, pp. 77–85, 1985.
[14] W. Elenbaas, “The dissipation of heat by free convection the inner surface of vertical tubes of different shapes of cross-section,” *Physica*, vol. 9, pp. 865–874, 1942.
[15] K. Ramakrishna, S.G. Rubin and P.K. Khosla, “Laminar natural convection of air along vertical square ducts,” *Numer. Heat Transf.* vol. 5, no. 1, pp. 59–79, 1982.
[16] K.T. Lee, “Laminar natural convection heat and mass transfer in vertical rectangular ducts,” *Int. J. Heat Mass Transf*. vol. 42, no. 24, pp. 4523–4534, 1999.
[17] T. Aihara, *Cooling Techniques for Computers*, Hemisphere, New York, 1991.
[18] G.D. Raithby and K.G.T. Hollands, *Handbook of Heat Transfer*, 2nd ed., McGraw–Hill, New York, 1985.
[19] M.M. Yovanovich, P. Teertstra, and Y.S. Muzychka, “Natural convection inside vertical isothermal ducts of constant arbitrary cross-section,” *J. Thermophy. Heat Transf.* vol. 16, no. 1, pp. 116–121, 2002.
[20] T. Yilmaz and S.M. Fraser, “Turbulent natural convection in a vertical parallel-plate channel with asymmetric heating,” *Int. J. Heat Mass Transf*. vol. 50, pp. 2612–2623, 2007.
[21] M. Abdollahzadeh, M. Esmaeilpour, R. Vizinho, A. Younesi, and J. C. Pàscoa, “Assessment of RANS turbulence models for numerical study of laminar-turbulent transition in convection heat transfer,” *Int. J. Heat Mass Transf*. vol. 115, pp. 1288–1308, 2017.
[22] C.E. Clifford and M.L. Kimber, “Assessment of RANS and LES turbulence models for natural convection in a differentially heated square cavity,” *Numer. Heat Transf. A*, vol. 78, no. 10, pp. 560–594, 2020.
[23] D. Chatzikyriakou, J. Buongiorno, D. Caviezel, and D. Lakehal, “DNS and LES of turbulent flow in a closed channel featuring a pattern of hemispherical roughness elements,” *Int. J. Heat Fluid Flow*, vol. 53, pp. 29–43, 2015.